

Clinical Pneumonia Classification Based on Multimodal Data Fusion

Abstract. Existing CAD(Computer Aided Detection) systems for pneumonia diagnosis are basically designed for X-ray image. But in clinical application, CT(Computed Tomography) has become the most common technology for diagnosing pneumonia. But applying deep learning directly to raw CT scans requires much resource of computing. Moreover, patients' personal complaints are often ignored, which are very important in clinical diagnosing. In this study, we propose a novel model, MMD-D(Multimodal Data Diagnosis), which combines CT visual features with patients' age, gender and complaints. In MMDD, we treat process of reading CT scans as playing short videos and transform analyzing CT scans into analyzing videos, so a RCNN(Recurrent Convolutional Neural Network) is used to capture visual features from CT image data. Meanwhile, complaints will be transformed into word vectors by word2vec and analysed by LSTM. Visual features and complaint textual features will be fused together with patients' age and gender. All information above will play a role in the decision making process. We extract images from three different attention from CT scans and transform 1-channel grey level CT images into 3-channel false color RGB images. Moreover, we use a auxiliary loss to train CNN properly. Our model achieves 0.945 in accuracy, and has a very balanced performance in sensitivity and specificity. As far as we know, we are the first to classify pneumonic cases based on large scale clinical raw data using multimodal data.

Keywords: Long Short Term Memory(LSTM) · Pneumonia Diagnosis · Convolutional Neural Network · Computed tomography (CT) · Computer-aided detection and diagnosis (CAD) · Multimodal Data

1 Introduction

Chest X-rays used to be the best available method for diagnosing pneumonia, playing a crucial role in clinical care[1] and epidemiological studies[2]. However, with the development of economic, CT(Computed Tomography) has become the most common technology for diagnosing pneumonia in China. According to the survey, a radiologist of the major hospital need to read hundreds scans of CT every day. Thus, developing a fast, robust and accurate CAD system to perform automated diagnosis of pneumonia is meaningful and important.

There have been lots of models designed for diagnosing thoracic diseases. Hoo-Chang Shin [3] combined CNN and LSTM[4], proposed a model which can describe the contexts fo a detected diseases based on the deep CNN features. This model used CNN to extract features from chest X-Ray and used LSTM

to generated MeSH[5] terms for chest X-Ray. In 2017, Xiaosong Wang et al.[6] provided hospital-scale chest X-ray database ChestX-ray8 which contains eight common thoracic diseases. This database allow researchers use deeper neural network to analyze medical images. Based on this dataset, Pranav Rajpurkar, Andrew Y. Ng et al. [7] developed CheXnet with 121-layer. This model achieved an F1 score of 0.435, higher than human radiologists. Later in 2018, Xiaosong Wang et al.[8] proposed TieNet, which can classify the chest X-Rays into different diseases and generate the report at the same time. In TieNet, CNN was used capture features of chest X-Rays, RNN learned these features and generate report based on attention mechanism, which can help model to focus on different parts of chest X-Ray alone with the generation of reports.

Studies above have something in common. First of all, they were designed for chest X-Rays, which means these methods can only handle 2D images. Even if models can achieve good results in every indication, these models still cannot handle CT(Computed Tomography) scans, which is commonly used in clinical practice. Compared with X-Rays, CT scans contain much more complex information. Each slice in CT scans is a 2-D image of human body, using these 2-D slices can reconstruct 3-D structure of human bodies. Moreover, CT scans have a more clear view of patients' bodies, since ribs and clavicles won't cast shadows in front of chest. As a result, CT scans have a much larger data size. One series of chest CT contains hundreds of slices and each slice has a size of 512×512 . Extensive studies show that 3-D CNN is the best choice for keeping 3D spatial information in the CT scans [9]. However, 3-D CNN cannot be applied to raw CT data directly since it will bring a heavy burden to the server. Moreover, because of specific characteristics of medical images, we cannot reduce the size of data by resizing or splitting images.

Second, for models designed for diseases diagnosing like CheXnet, few of them combine image visual features with other information about patients like gender, age. For models like TieNet, they combine image visual features with descriptions written by radiologists, but descriptions from radiologists are only related to images, this descriptions only help models understand image without knowing anything about patients themselves, which is contrary to the clinical diagnosis process. Patients' complaints is a very useful information when doctors are diagnosing, because complaints is patients' direct feeling about their physical condition. However, as far as we know, few studies use this information to improve the performance of CAD systems.

In general, there are two major problems of existing CAD systems: 1, they cannot handle CT scans and analyze 3-D information, and this problem has become a practical limitation of deep learning models designed for medical problems; 2, they only analysis visual features of medical images, but seldom consider patients' feeling and personal information.

In this study, we treat slices of CT scans as video frames, and transform the problems of classifying CT scans into the problems of classifying videos. We use RCNN(Recurrent Convolutional Neural Network) to extract features from slices of CT scans. Moreover, we embed patients' complaints into word

vectors using word2vec[10][11] and use LSTM(Long Short Term Memory) to extract textual features, and concatenate it with features of images, along with information about patients' age and gender. All information above will be fused and analysed by MMDD(Multimodal Data Diagnosis) model. Our model achieve 0.945 in accuracy and 0.9358 in sensitivity.

The remainder of the manuscript is organized as follows. Section 2 describes the data and steps of pre-processing. Section 3 describes the architecture of MMDD and details of our model. Section 4.2 reports our experiments results and discussion of experiments. Our conclusions is listed in section 5.

2 Data

2.1 CT Image Data and Multimodal Data

Because the shortage of public CT dataset for pneumonia, we use raw data from a major hospital. We get 1036 cases of CT(842 cases with pneumonia, 464 healthy cases) from hospital PACS(Picture Archiving and Communication Systems). Open a CT scan with RadiAnt DICOM Viewer¹, as shown in Fig 3, we can see that raw data from hospital may have more than one series of images(yellow rectangle), each series may have different data type or different image windows. Doctors or radiologists may read details of images from main area of reader(red rectangle), but for deep learning models, they have to learn information from data with consistent data form. As a result, we have to pick up the most suitable series from raw data. This work is very heavy, so we design a protocol to let the computer pick up data for us.

First of all, we eliminate these cases which start scanning from the middle of the chest. Then we pick up the best series from the whole cases according to the following requirements:

1. We use the series with the specific 'Convolution Kernel'. Specific 'Convolution Kernel' can make the CT more suitable for observing the lungs or chest, for example, in Fig 2, slice under 'B70s' has clearer view of lungs, slice under 'B41s' has clearer view of heart. We choose 'B31f', 'I31f 3', 'B70f', 'B80f', 'B70s', since radiologists use these 'Convolution Kernels' more frequently to observe the lungs and chest than other kinds of 'Convolutional Kernel'. Number of different 'Convolution Kernel' is shown in Fig 1. However, different 'Convolution Kernels' will not affect images we analysis in the end, because all slices will be calculated and transformed into HU unit, which will be discussed in section 2.2.

2. We calculate 'Slice Thickness' of each series, and keep series with the smallest 'Slice Thickness', since small thickness may keep more detailed information of body structure.

3. If there were more than one series meet the last two requirements, we will keep the series with the largest number of scans, which can have a larger span of view.

¹ www.radiantviewer.com

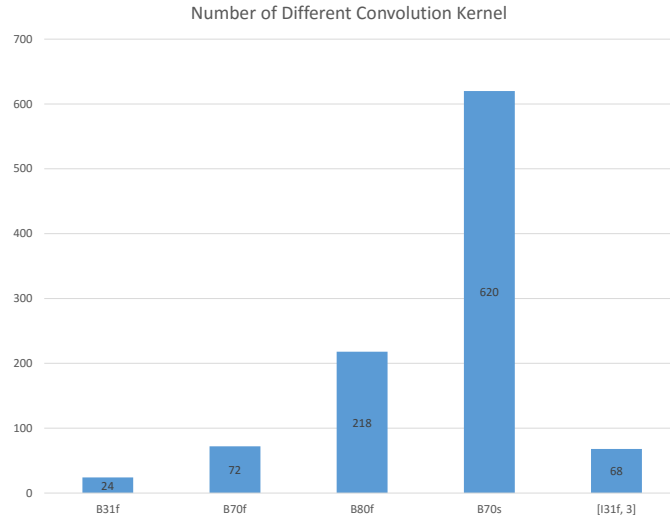


Fig. 1. Number of Different Convolution Kernel

As a result, we keep 552 cases with pneumonia and 450 cases of healthy people (1002 cases total). We split dataset in training/validation/testing as 60% /20% /20% and make them identically distributed in three parts of datasets, so we have 602 cases in training set, 200 cases in validation set, 200 cases in test set. Number of healthy and pneumonic cases in different slice-thickness is shown in Table 1.

Each CT scan has a case file. In case files, we can get patient basic information: patient ID, gender, age. Moreover, each case file contains patient complaint. Patient complaints are descriptions from patients which describe their own feeling about their condition, which is very important in clinical practice. In this study, we will use gender, age as additional features, and use LSTM extract features from patients' complaints, and combine them with features from CT scans.

2.2 Data Preprocessing

CT Image Data There are kinds of image windows for CT reader, such as windows for bone, brain, chest, lungs. Images under different image windows will highlight different tissues of bodies. As mentioned in section2.2, there kinds of 'Convolution Kernel' within different CT scans. Each kind of 'Convolution Kernel' in fact can show specific window for CT images directly from raw data. But it may make data inconsistent. So we transform raw data into HU(Hounsfield Unit) values. The Hounsfield Unit named after Sir Godfrey Hounsfield, is a quantitative scale for describing radio-density, its value is also termed CT number.

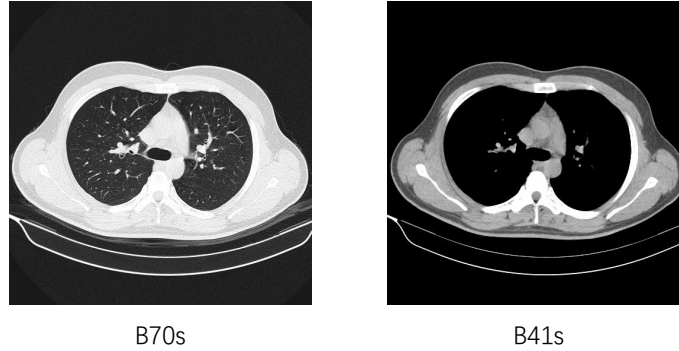


Fig. 2. Scans with Different Convolutional Kernel

Table 1. Number of Healthy and Pneumonic Cases in Different Slice-Thickness

<i>Slice-Thickness</i>	<i>Healthy</i>	<i>Pneumonic</i>
1 mm	0	24
1.5 mm	1	7
2 mm	444	386
3 mm	0	127
5 mm	5	8
Total	450	552

After transformed into HU values, all slices from CT scans will have the same unit of measure, then we will transform scans according to specific rules.

Following the study in [12] [13], we transform slices into images by using three HU range: normal[-1000, 400HU], high attenuation [-160, 240HU], low attenuation [-1400, -950HU]. In Fig4 we can see that, compared to original CT image, image in ‘Normal’ is brighter, tissues in lungs are clearer and details are enhanced. Image in ‘High Attenuation’ have a clear view of hearts and vessels(in yellow rectangle). ‘High Attenuation’ range also enhance the difference between high density pathological tissues(in white rectangle) and normal tissues. ‘Low Attenuation’ range highlight abnormal voids in lungs(in red rectangle) which is features of severe lung diseases. All images mentioned above are one-channel grey level images, and we finally combine three ranges images into 3-channel images which fits the requirements of CNN models. As shown in Fig 4, these 3-channel images are actually false color images. The ‘Slice Thickness’ between each slice is adjusted into 10mm, and each scan will keep 32 slices. The influence of different range will be discussed in section 4.2.

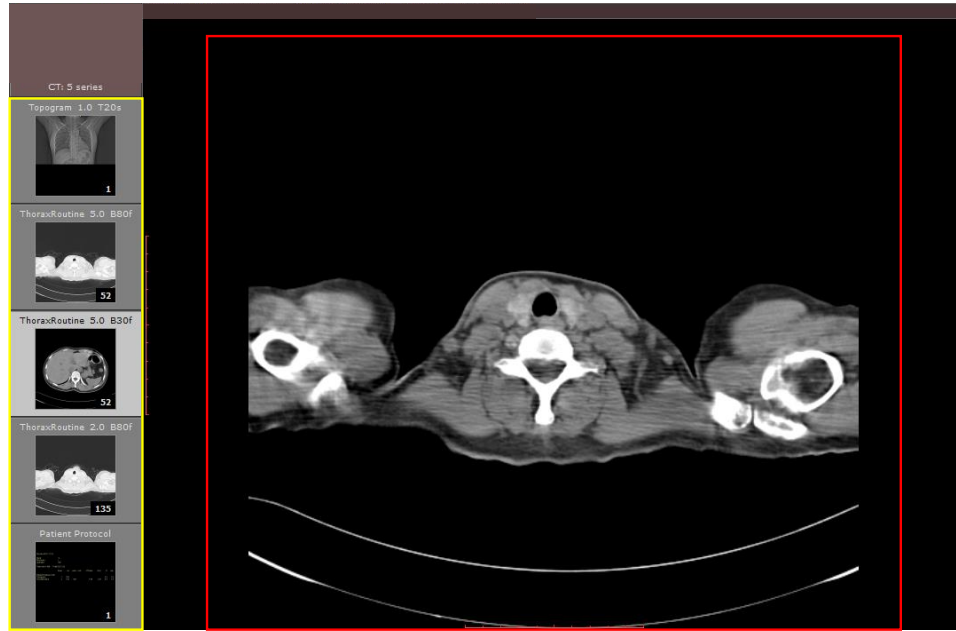


Fig. 3. Structure of Raw Data from Hospital

Patient Age, Gender and Complaints The pre-process of age, gender and complaints is shown in Fig 5. For each patient, we have a list of information contains age, gender and complaints. For patient age and gender, we transform them into numbers. Gender information will be transformed into a two-dimensional array, $[1, 0]$ represents male, $[0, 1]$ represents female. Age will be calculated according to patient birthday. For example, patient in 5 is an adult male, who was born in 1999-10-29. His gender and age will be transformed to $[1, 0]$ and 20.

For patients' complaints, since we only have Chinese complaints, we have to do Chinese word segmentation. Chinese word segmentation is a very difficult problem so we will take a short cut. We use a mature tools: Jieba text segmentation² to segment Chinese sentences into Chinese word sequences so that LSTM can analysis them. Before segmentation, we remove numbers, punctuation marks in order to get a better segmentation results. An example of Chinese word segmentation is shown in green rectangle in Fig 5. However, English patient complaints have no need to do segmentation. If you use data from English speaking countries, you may skip this step. After segmentation, we use word2vec to embed word sequences into vectors. We use CBOW(Continuous Bag-of-Words)[10] to capture relationship between words. Since our corpus is very small, we set embedding size as 50, and window size for CBOW as 3. In order to simplify model, we set length of Chinese word sequence to 16 since 16 is

² <https://github.com/fxsjy/jieba>

the maximum length among all complaint sequences. For those sequences whose length is less than 16, we add ‘None’ to fill up the voids and increase length to 16. The details of word2vec will not be discussed here. After embedding, each word will be embedded into a vector of 50 dimensions.

Code for data preprocessing will be released very soon. But we cannot release dataset because of the privacy of patients. We will release model with trained parameters and some sample data for demo.

3 Method

3.1 Recurrent Convolutional Neural Network

RCNN(Recurrent Convolutional Neural Network) has been proved to be very useful for video caption, description and classification [14][15], however, only a few work apply RCNN to medical image analysis. Zreik, Majd et al. [16] recently use RCNN for automatic detection and classification of coronary artery plaque, they use CNN extracts features out of $25 \times 25 \times 25$ voxels cubes, and use an RNN to processes the entire sequence using gated recurrent units (GRUs). They prove that RCNN’s potential for sequence information processing of medical images.

Follow the study[14], we use LSTM as our RNN cells cause LSTM has been demonstrated to be capable of large-scale learning of sequence data. However, few studies have paid attention to different CNN models’ performance on medical images, so we try three kinds of classic CNN models: VGG[17], ResNet[18] and Inception-V3 [19]. Experiments show that ResNet50 has the most stable performance, so that we use ResNet50 as feature extractor of images. Moreover, we wanted to test deeper models like ResNet101, but it will cost more resource of calculation, so we still keep ResNet50. In order to get best combination between CNNs and LSTM, we test different combinations with images under different ranges of HU value, which will be discussed in section 4.2.

We use ResNet50 without fully connected layers as feature extractor. Fig 6 shows the architecture of ResNet50 blocks. As we all know, block provide short-cut connection between input and outputs of three convolutional layers and allow us to build very deep CNN model.

The input size of CNN is 512×512 , so the outputs of CNN will be $16 \times 16 \times 2048$. If we use fully-connected layer, the length of first fully-connected layer will be 1×524288 , which will make this model very difficult to train. So we use global average pooling proposed in study[20], as shown in Fig 8, which is a replacement of fully-connected layers to enable the summing of spatial information of feature maps, and reduce the greatly reduce the number of neurons. After global average pooling, feature maps from CNN will be reshaped into a tensor of size 1×2048 , then we use a fully-connected layer to reduce this tensor to 1×256 . If we have n slice, we will have a matrix with size $n \times 256$, this matrix will be fed into LSTM by n steps. Our input images are actually false color RGB images, so the number of LSTM units is set to 256 following study in [14]. In order to get the best RCNN for CT scans, we run experiments to get the best combination

between CNNs and LSTM. The experiments show that ResNet50 performs the best in these three models, so our RCNN use ResNet50 as its CNN part, and use one layer of LSTM as its RNN part. In fact, LSTM layer plays the role of encoder, it encodes image feature sequences and gives out the output of the last step as middle state hv_t :

$$hv_t = LSTM(Fx_t, hv_{t-1}, z_{t-1}) \quad (1)$$

Fx_t is the t -th visual features in CT slices, hv_{t-1} is LSTM hidden state of $t - 1$ step, z_{t-1} is LSTM output of $t - 1$ step. t is the length of slices, in this study, t is equal to 32.

3.2 Multimodal Data Fusion and MMDD

Besides CT image information, we also know patients gender, age, and complaints. For gender and age, we use them as additional features and set two tensors with size 1×1 to hold them. For patients' complaints, as mentioned in section 2.2, we will use Jieba Chinese word segmentation tool to segment Chinese sentences into word sequences. We set length of Chinese word sequence to 16. Then we transform sequences of words into sequences of vectors using word2vec, which is commonly used in nature language process, since it can capture the relations between words. The width of vectors is set to 50, so does the number of LSTM units. This LSTM is the second encoder to encode complaint. It is calculated in the same way as equation 1:

$$hc_{ct} = LSTM(Cx_{ct}, hc_{ct-1}, z_{ct-1}) \quad (2)$$

Cx_{ct} is word embedding matrix of the ct -th word in complaint, hc_{ct-1} is LSTM hidden state of $ct - 1$ step. ct is the length of complaint, which is 16.

We use cross-entropy as classification loss function[16]. After getting hv_t , hc_{ct} , we can calculate the prediction and loss as follows:

$$\begin{aligned} loss1 &= \sum_i y_i \log(\Delta_i), \\ \Delta &= Softmax(F(hv_t \otimes hc_{ct} \otimes A \otimes G)) \end{aligned}$$

where y_i are vectors for the labels of patients, Δ is prediction after Softmax, \otimes is the concatenation operation, F is a function to fuse hv_t , hc_{ct} , A and G , in this study, we simply use two fully-connected layers to fit the function. A is patient age, G is patient gender.

Since LTSM need to encode 32 visual features, we assume that the gradients propagate to CNN will be very small, so that CNN will not be trained properly. Invoked by study in [19], we use a auxiliary loss to enhance signal of gradient for CNN. The auxiliary loss is defined as follow:

$$\begin{aligned} Loss &= (1 - \omega) \times loss1 + \omega \times loss2 \\ loss2 &= \sum_i y_i \log(\Delta_i^c) \end{aligned}$$

where ω is a parameter within the interval $(0, 1)$. $loss2$ is classification cross-entropy loss from CNN, Δ_i^c is Softmax prediction of CNN. ω can adjust the weight of two losses at different training phases. We expect that at the beginning of training, CNN get stronger gradient and learning to capture features from CT images more quickly. After parameters of CNN get stable, $loss1$ tends to get small and keep updating parameters of LSTM. We output weights of two losses during training MMDD, as shown in Table 2, weight for LSTM loss($1 - \omega$) is 0.6238 at the beginning of training(602 steps), however, W1 will increase to 0.7234 when training process comes to 36120 steps, it meas weight for CNN is 0.3762 at 602 steps, and it will drop to 0.2766 at the end. Experiments also show that RCNN with auxiliary loss can have a better performance, which will be discussed latter in section 4.2.

Finally, a Multimodal Data Diagnosis(MMDD) is built, RCNN for image data and LSTM for complaints will be trained jointly, the architecture of MISD is shown in Fig 9. Model will be trained for 4 epoch, and each epoch contains 15 iteration for all training data.

Table 2. Weights of Two Losses at Different Training Step

<i>Number of Steps</i>	$1 - \omega$	ω
602	0.6238	0.3762
9030	0.6547	0.3453
18060	0.7027	0.2973
27090	0.7185	0.2815
36120	0.7234	0.2766

There two steps during training process. The first step is to train difference kinds of RCNN to get the best combination between CNNs and LSTM, the outputs from RCNN(1×256) will be feed into two fully connected layers to get classification results, as shown in Fig 7. We compare three kinds of classic CNN models: VGG16, GoogleNet with Inception-V3, ResNet50. VGG16 is relatively shallow, ResNet50 is deepest in these three kinds of models. We tried to use deeper network like ResNet101, however using ResNet101 make the training of model very slow and bring a heavy burden to servers. So we keep ResNet50 in RCNN.

The second step is to train MMDD model. We use model get in the first step as encoder for CT scan visual features, use LSTM as feature encoder for complaints, and combine them with information of age and gender. All these features will be feed into two fully-connected layers to get final classification results.

Moreover, we use CNN models pre-trained on ImageNet[21]. Models without pre-training is almost impossible to train because it won't converge or converge very slow during training. We test difference RCNNs, and experiments show

that using pre-trained models can significantly improve the converging speed, as shown in Fig 3.

Table 3. Comparison between training from scratch and training with pre-trained weights

<i>Structure</i>	<i>Pre-trained</i>	<i>Data</i>	<i>Accuracy</i>	<i>Sensitivity</i>	<i>Specificity</i>	<i>AUC</i>
RCNN(ResNet)	No	Normal	0.545	1.0	0.0	0.57
RCNN(GoogleNet)	No	Normal	0.545	1.0	0.0	0.5
RCNN(ResNet)	Yes	Normal	0.925	0.954	0.890	0.922
RCNN(GoogleNet)	Yes	Normal	0.865	0.826	0.912	0.869

Initial learning rate is set 0.0005 and drops 50% every 3000 training steps. The dropout rate in fully-connected layers is set to 0.5.

4 Experiments and Results

4.1 Effectiveness of 3-Channel

In order to verify the effectiveness of 3-channel pre-process, we output the feature maps of convolutional layer with 3-channel images, normal images, high attenuation images and low attenuation images. As show in Fig 10. In order to keep inconsistent of experiments environment, all experiments carried on in this part is based on ResNet. The first column is original CT images, which is direct output from CT slices. The second column is 3-channel original images, which combine 3 difference ranges of HU values. The last four columns are feature maps with normal image, high attenuation image, low attenuation image. The first four rows are pneumonic cases, and the last case is healthy case.

Compared to original CT images, we can clearly see that 3-channel images can show more density information about lung tissues. Original CT images are actually grey level images, which can only show lungs with white, black or grey. In this modal, high dense tissues are white, normal lung tissues and low dense tissues are tend to be black. If you want to see details of low dense tissues, you have to adjust the window to low attenuation range, but meanwhile you will lost the details of high dense tissues. In 3-channel images, details of high dense and low dense tissues will both be kept. We can see images in the second columns have a larger scale of colors. First of all, high dense tissues will still tend to be white, like bones, high dense tissues in lungs. Second, normal lung tissues will tend to be red, low dense tissues tend to be black, which is very useful when patients have severe lung diseases. For example, in the first row, lungs in this case has a very large void space, but in original CT images, this void is not very obvious since other normal tissues is in black color too. But in 3-channel image, we can clearly notice the difference between normal tissues and low dense tissues. Moreover, the details of high dense tissues are still kept.

To verify the effectiveness of difference ranges of HU values, we output middle feature maps of ResNet. More specificity, we output the feature maps after one

convolutional layer, one max pooling layer, and three blocks, which have 256 channels, the size of feature maps are 128×128 , then we resize them into 512×512 . We can see that CNN trained by 3-channel images has advantages over CNNs trained by other images. In the first and the second rows, 3-channel CNN can capture the low dense tissues of lungs, which are not very clear in visual. Low attenuation CNN can notice the low dense tissues, but apparently the details of heart and vessels are ignored in the last column. In high attenuation CNN and normal CNN, low dense tissues have no significant difference compared to normal lung tissues. In the third and the forth row, 3-channel CNN still has ability to capture high dense tissues, which is the same as normal CNN and high attention CNN, but low dense CNN has difficulty in doing this. In the third row, low attenuation CNN cannot distinguish the normal and unnormal tissues. However, in the forth row, low attenuation CNN simply ignores high dense tissues. The last row shows a healthy case. Healthy case has a clear view in the first four columns, but shows nothing in low attenuation CNN.

4.2 Validation

In order to prove the effect of CNN, auxiliary loss and Multimodal Data, we run a lot of experiments to compare with each other, and the results of experiments is shown in Table 4.

First of all, we do experiments to prove the effect of images with three ranges of HU values. We can see that RCNN(ResNet), RCNN(GoogleNet) and RCNN(VGG) trained by three channel image all have better performance than these models trained by one channel data. For RCNN(VGG), model trained by three channel image outperforms RCNN(VGG) trained by Normal Image in accuracy, specificity and AUC score. Even if RCNN(VGG) with Normal Image has better performance in sensitivity, we can see that it only get 0.626 in specificity, which means this model is not been trained well. For RCNN(ResNet) and RCNN(GoogleNet), we can see that these two models trained by Three Channel Image perform best compared to models trained by Normal Image, High Attenuation Image and Low Attenuation Image. Especially RCNN(ResNet) trained by Three Channel Image, it get 0.93 in accuracy, 0.934 in specificity, 0.93 in AUC score, which are highest in six versions of experiments. RCNN(ResNet) trained by Normal Image has 0.954 in sensitivity, which is the highest in six experiments, but it only achieve 0.824 in specificity, which corrupts the performance of whole model. As a result, we use RCNN(ResNet) as our visual feature encoder for CT.

Then we run a experiment to prove the effectiveness of auxiliary loss. We train RCNN(ResNet) with three channel image, but we set ω to 1, which means we remove the gradient propagates directly to CNN and the model actually has only one loss. We can see that the performance of RCNN with single loss drops around 1% in all four indication. It proves that, by using auxiliary loss, CNN will be trained in a better way.

At last, we run experiments to prove than Multimodal Data can enhance the performance of CAD system. As shown in section 9, the output of RCNN($1 \times$

256), features of complaints(1×50), gender(1×1) and age(1×1) will be concatenated together(1×308) and fused by two fully-connected layers. It is simple, but effective. We can see that MMDD has the highest score in accuracy, specificity and AUC score. But it achieves 0.936 in sensitivity, 1.8% lower than the highest 0.954. It means MMDD has the best performance of binary classification according to its AUC score. We also remove the information about age and gender, we found that MMDD without age and gender have similar performance compared to RCNN(ResNet), MMDD without age and gender has a higher score in sensitivity and lower score in specificity. Compared to MMDD without information about gender and age, MMDD with multimodal data has better performance in accuracy, specificity and AUC, but slightly lower in sensitivity.

Table 4. Comparison of All Kinds of RCNN and MMDD

<i>Structure</i>	<i>Data</i>	<i>Accuracy</i>	<i>Sensitivity</i>	<i>Specificity</i>	<i>AUC</i>
RCNN(VGG)	Normal	0.805	0.954	0.626	0.790
RCNN(VGG)	Three Channel	0.890	0.927	0.846	0.886
RCNN(GoogleNet)	Normal	0.865	0.826	0.912	0.869
RCNN(GoogleNet)	High Attenuation	0.880	0.853	0.912	0.883
RCNN(GoogleNet)	Low Attenuation	0.860	0.890	0.824	0.857
RCNN(GoogleNet)	Three Channel	0.905	0.900	0.912	0.906
RCNN(ResNet)	Normal	0.925	0.954	0.890	0.922
RCNN(ResNet)	High Attenuation	0.875	0.908	0.835	0.872
RCNN(ResNet)	Low Attenuation	0.865	0.900	0.824	0.861
RCNN(ResNet), One Loss	Three Channel	0.920	0.917	0.923	0.920
RCNN(ResNet)	Three Channel	0.930	0.927	0.934	0.930
MMDD	CT & Textual Data	0.925	0.945	0.901	0.923
MMDD	Multimodal Data	0.945	0.936	0.956	0.945

The validation loss and accuracy during training is shown in Fig 11 and Fig 12. We can see that In Fig 11, MMDD can achieve higher accuracy at the first phase of training, but RCNN(ResNet), RCNN(GoogleNet) and RCNN(ResNet) with single loss perform better after. MMDD's performance outperforms other methods again after 27000 training step. It is not hard to understand this phenomenon. Because MMDD considers patients' information about age, gender and complaints, it can achieve about 0.70 in accuracy at the first training phase. But other methods has less parameters to be optimized, so they converge more quickly than MMDD. We can also see RCNN(ResNet), RCNN(ResNet) with single loss have similar performance during training, but RCNN(ResNet) with auxiliary loss perform a little bit better than RCNN(ResNet) with single loss at the end of training. For RCNN(GoogleNet), it converge slower than RCNN(ResNet) and RCNN(ResNet) with single loss, and has a lower accuracy in the end. Without age and gender, MMDD has similar performance compared to RCNN(ResNet) with single loss. It means, in this dataset, age and gender have significantly influence on model.

The phenomenon shown in Fig 12 is also can be explained. RCNN(GoogleNet) has the highest loss at the end of training, so it perform the worst in accuracy. RCNN(ResNet) and RCNN(ResNet) Without age and gender, MMDD has similar performance compared to R with single loss have the similar loss. MMDD's loss decrease steadily, even if it has the highest loss for a moment during training, but it has the lowest loss after 27090 training steps. MMDD without gender and age has similar performance compared to RCNN(ResNet).

According to the experiments above, we can see that information about age and gender can improve accuracy to 0.7 at the very beginning, it means the dataset we are using must be influenced by some certain distribution. So we count the number of male patients and female patients in healthy cases and pneumonic cases(Table 5) and number of patients in different ages(Table 6).

In Table 5, we can see that a male patient has a larger chance of being pneumonic. In 601 male cases, about 60% of them are pneumonic, however, in 401 female cases, only 47.6% are pneumonic. This may be related to smoking since male in China suffer a serious smoking problem. In Table 6, we can see that age is also related to the chance of being pneumonic. We have to notice that people turn to hospital or clinic may have noticed that something went wrong about their healthy condition, but we can still see that people older than 40 have much larger chance of being pneumonic. There are about half of healthy cases between 40-50, but this number drops so quickly that it goes down to 28.8% between 50-60. It is not hard to understand this phenomenon, since young people are very sensitive about their healthy condition, they will go to have physical examination as long as they feel uncomfortable, even if they have a lower chance of have pneumonia. However, old people have to face up with another condition. Most old people only go to hospital or clinic when their conditions are very bad. It remind us that there is a lot of work about old people health care.

Table 5. Number of Male and Female Patients in Healthy and Pneumonic Cases

	<i>Healthy</i>	<i>Pneumonic</i>	<i>Total</i>
Male	240	361	601
Female	210	191	401
Total	450	552	1002

5 Conclusions

In this study, we propose a novel model, MMDD(Multimodal Data Diagnosis), which combines CT visual features with patients' age, gender and complaints. In MMDD, CT scans will be treated like videos, and analysed by RCNN(Recurrent Convolutional Neural Network), complaints will be transformed into word vec-

Table 6. Number of Healthy and Pneumonic Cases in Different Ages

	<i>Healthy</i>	<i>Pneumonic</i>	<i>Total</i>
0-10	6	1	7
10-20	31	2	33
20-30	122	30	152
30-40	124	45	169
40-50	109	108	217
50-60	53	131	184
60-70	5	126	131
70-80	0	82	82
> 90	0	27	27
Total	450	552	1002

tors by word2vec and analysed by LSTM. Features from CT images and complaints will be fused together with patients’ age and gender. All these features will be used to classify cases into healthy cases or pneumonic cases.

We analyze 1002 cases(450 healthy cases and 552 pneumonic cases). In fact, 1002 cases is far small than ‘big data’, so our model’s performance is restricted by data distribution and quality. However, in clinical practice, it is very difficult to construct a big scale medical dataset for deep learning, cause raw data is affected by radiologists’ personal habits, data acquisition equipments, and hospital work rules. Our future work will focus on methods of data pre-processing which can over come difficulties mentioned above. Moreover, our future work will also focus on fusing more source of information, like medical history, family history, blood test and other information witch will be considered during clinical practice. All works above will be carried out under the premise of respecting the privacy of the patients.

References

1. Franquet T. Imaging of pneumonia: trends and algorithms. *European Respiratory Journal*, 18(1):196–208, 2001.
2. Thomas Cherian, E Kim Mulholland, John B Carlin, Harald Ostensen, Ruhul Amin, Margaret De Campo, David Greenberg, Rosanna Lagos, Marilla G Lucero, Shabir A Madhi, et al. Standardized interpretation of paediatric chest radiographs for the diagnosis of pneumonia in epidemiological studies. *Bulletin of The World Health Organization*, 83(5):353–359, 2005.
3. Hoo Chang Shin, Kirk Roberts, Le Lu, Dina Demner-Fushman, Jianhua Yao, and Ronald M Summers. Learning to read chest x-rays: Recurrent neural cascade model for automated image annotation. In *Computer Vision & Pattern Recognition*, 2016.
4. Sepp Hochreiter and Jurgen Schmidhuber. Long short-term memory. *Neural Computation*, 9(8):1735–1780, 1997.
5. Mesh: Medical subject headings. <https://www.nlm.nih.gov/mesh/meshhome.html>.

6. Xiaosong Wang, Yifan Peng, Le Lu, Zhiyong Lu, Mohammadhadi Bagheri, and Ronald M Summers. Chestx-ray8: Hospital-scale chest x-ray database and benchmarks on weakly-supervised classification and localization of common thorax diseases. *computer vision and pattern recognition*, pages 3462–3471, 2017.
7. Pranav Rajpurkar, Jeremy Irvin, Kaylie Zhu, Brandon Yang, Hershel Mehta, Tony Duan, Daisy Ding, Aarti Bagul, Curtis P Langlotz, Katie Shpanskaya, et al. Chexnet: Radiologist-level pneumonia detection on chest x-rays with deep learning. *arXiv: Computer Vision and Pattern Recognition*, 2017.
8. Xiaosong Wang, Yifan Peng, Lu Le, Zhiyong Lu, and Ronald M. Summers. Tienet: Text-image embedding network for common thorax disease classification and reporting in chest x-rays. In *IEEE CVPR 2018*, 2018.
9. T. Yorozu, M. Hirano, K. Oka, and Y. Tagawa. Electron spectroscopy studies on magneto-optical media and plastic substrate interface. *IEEE Translation Journal on Magnetics in Japan*, 2(8):740–741, 1987.
10. Tomas Mikolov, Kai Chen, Greg Corrado, and Jeffrey Dean. Efficient estimation of word representations in vector space. *arXiv preprint arXiv:1301.3781*, 2013.
11. Tomas Mikolov, Ilya Sutskever, Kai Chen, Greg S Corrado, and Jeff Dean. Distributed representations of words and phrases and their compositionality. In *Advances in neural information processing systems*, pages 3111–3119, 2013.
12. Hoo-Chang Shin, Holger R Roth, Mingchen Gao, Le Lu, Ziyue Xu, Isabella Noguees, Jianhua Yao, Daniel Mollura, and Ronald M Summers. Three aspects on using convolutional neural networks for computer-aided detection in medical imaging. In *Deep Learning and Convolutional Neural Networks for Medical Image Computing*, pages 113–136. Springer, 2017.
13. Mingchen Gao, Ulas Bagci, Le Lu, Aaron Wu, Mario Buty, Hoo-Chang Shin, Holger Roth, Georgios Z Papadakis, Adrien Depeursinge, Ronald M Summers, et al. Holistic classification of ct attenuation patterns for interstitial lung diseases via deep convolutional neural networks. *Computer Methods in Biomechanics and Biomedical Engineering: Imaging & Visualization*, 6(1):1–6, 2018.
14. Jeffrey Donahue, Lisa Anne Hendricks, Sergio Guadarrama, Marcus Rohrbach, Subhashini Venugopalan, Kate Saenko, and Trevor Darrell. Long-term recurrent convolutional networks for visual recognition and description. In *Proceedings of the IEEE conference on computer vision and pattern recognition*, pages 2625–2634, 2015.
15. Nayyer Aafaq, Naveed Akhtar, Wei Liu, Syed Zulqarnain Gilani, and Ajmal Mian. Spatio-temporal dynamics and semantic attribute enriched visual encoding for video captioning. *arXiv preprint arXiv:1902.10322*, 2019.
16. Majd Zreik, Robbert W. Van Hamersvelt, Jelmer M. Wolterink, Tim Leiner, and Ivana Isgum. A recurrent cnn for automatic detection and classification of coronary artery plaque and stenosis in coronary ct angiography. *IEEE Transactions on Medical Imaging*, PP(99):1–1, 2018.
17. Karen Simonyan and Andrew Zisserman. Very deep convolutional networks for large-scale image recognition. *international conference on learning representations*, 2015.
18. Kaiming He, Xiangyu Zhang, Shaoqing Ren, and Jian Sun. Deep residual learning for image recognition. *computer vision and pattern recognition*, pages 770–778, 2016.
19. Christian Szegedy, Vincent Vanhoucke, Sergey Ioffe, Jonathon Shlens, and Zbigniew Wojna. Rethinking the inception architecture for computer vision. *computer vision and pattern recognition*, pages 2818–2826, 2016.

20. Min Lin, Qiang Chen, and Shuicheng Yan. Network in network. *international conference on learning representations*, 2014.
21. Olga Russakovsky, Jia Deng, Hao Su, Jonathan Krause, Sanjeev Satheesh, Sean Ma, Zhiheng Huang, Andrej Karpathy, Aditya Khosla, Michael Bernstein, Alexander C. Berg, and Li Fei-Fei. ImageNet Large Scale Visual Recognition Challenge. *International Journal of Computer Vision (IJCV)*, 115(3):211–252, 2015.

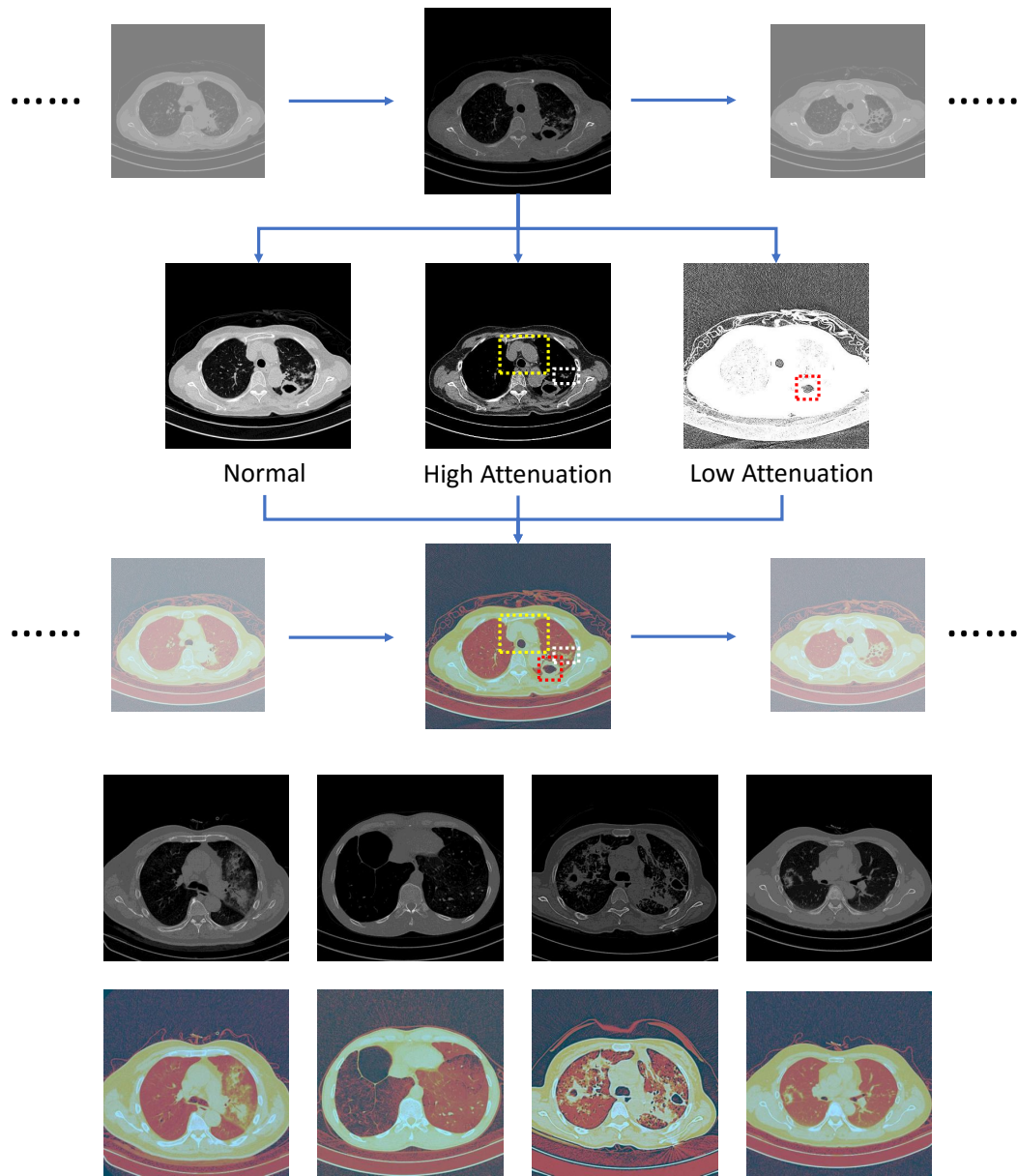


Fig. 4. Data Pre-process for CT Scans

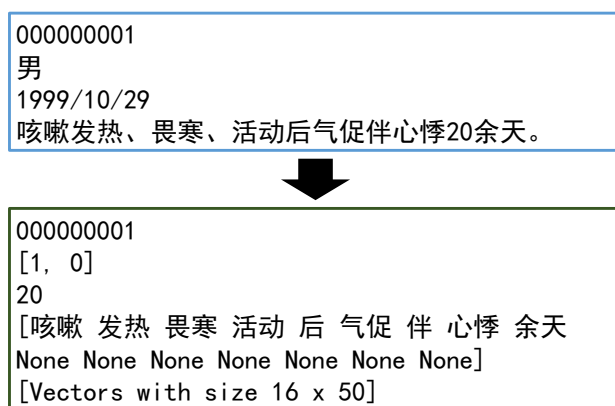
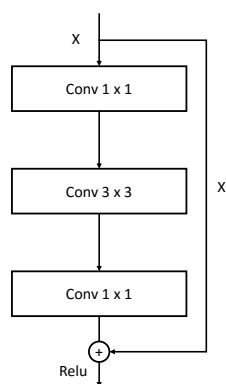


Fig. 5. Data Pre-precess for Age, Gender and Complaints

Fig. 6. Architecture of ResNet50 Block



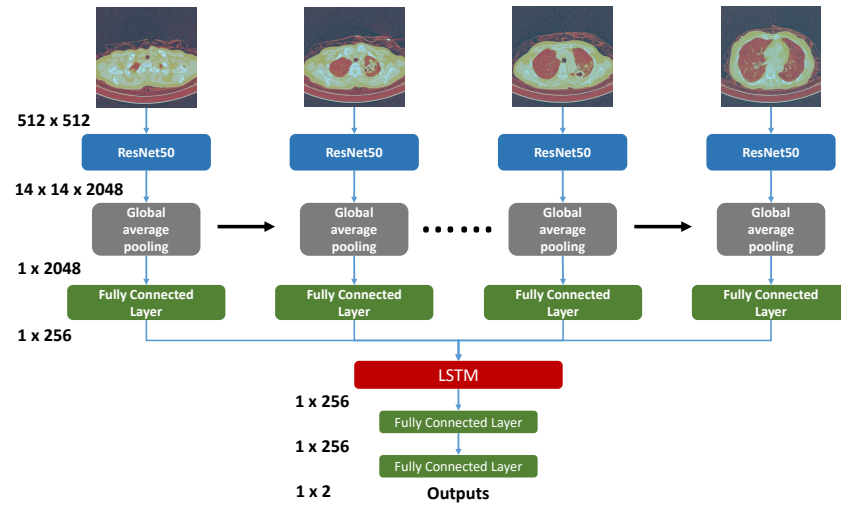


Fig. 7. Architecture of RCNN

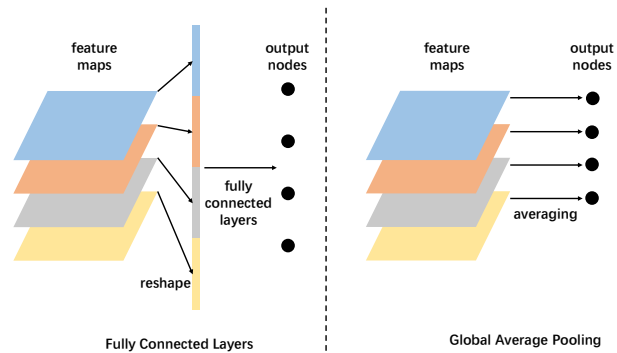


Fig. 8. Difference between Fully Connected Layers and Global Average Pooling

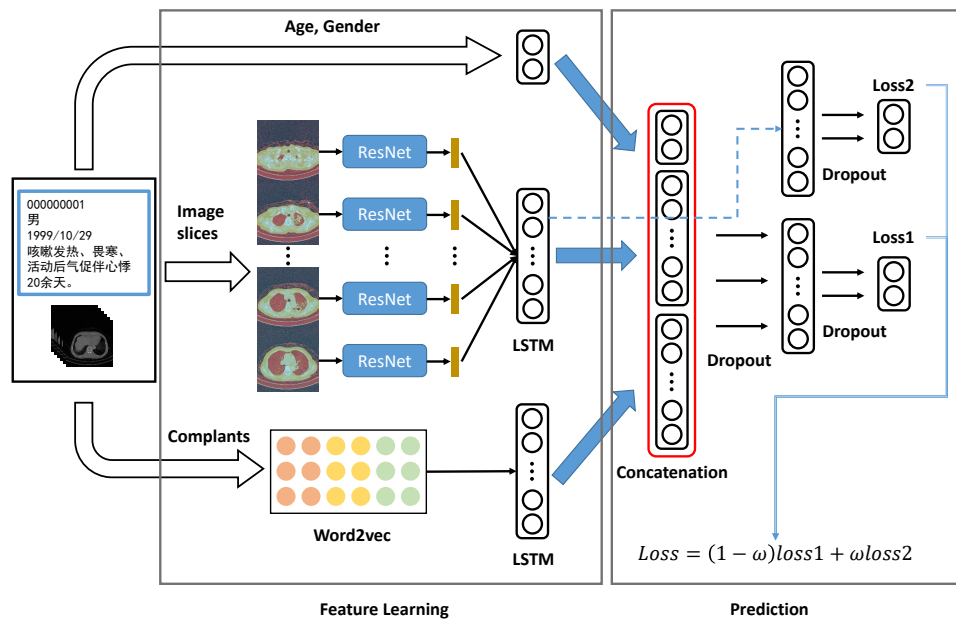


Fig. 9. Multimodal Data Diagnosis Model

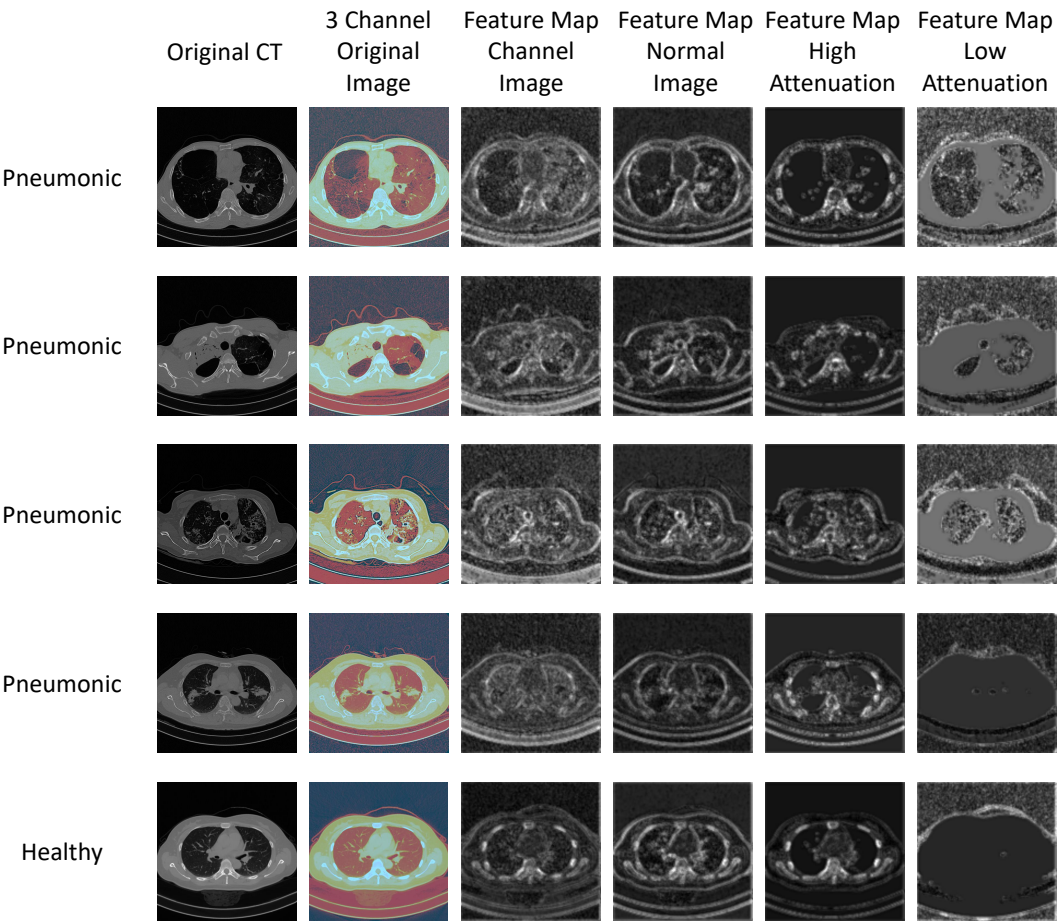


Fig. 10. Convolutional Feature Maps of Difference Types of Images

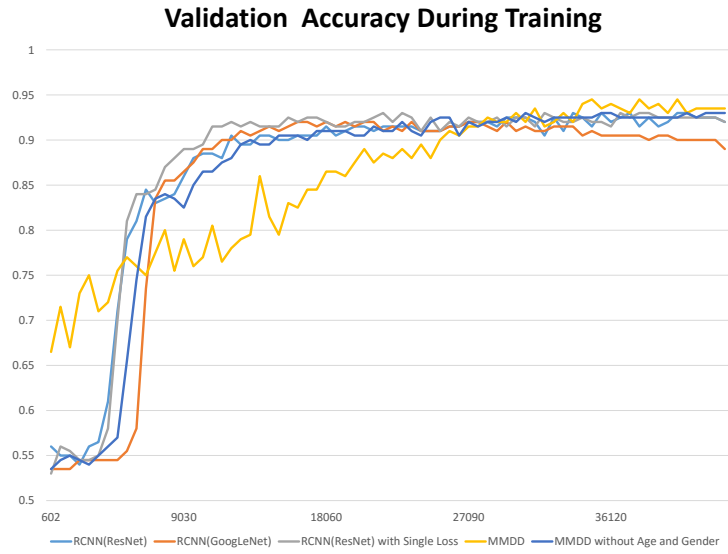


Fig. 11. Validation Accuracy During Training

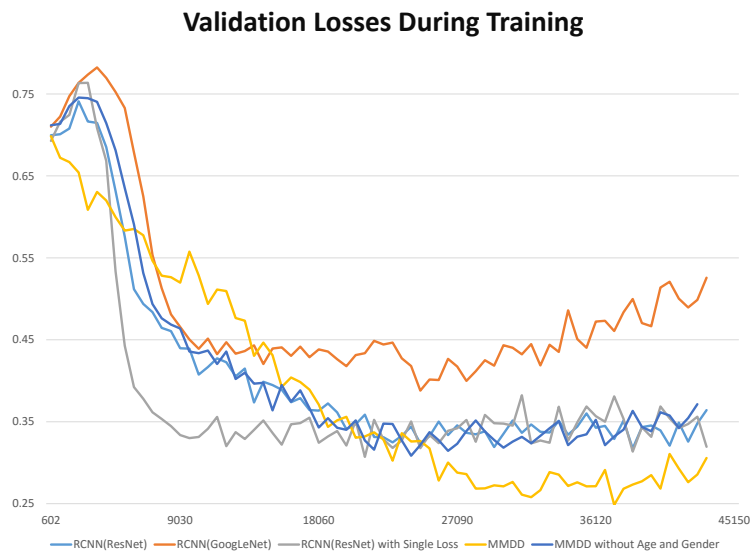


Fig. 12. Validation Loss During Training